

# Computer simulation of growth of duplex structures

K.M. CRUIKSHANK, K.E. NEAVEL and GUO ZHO ZHAO

*M. King Hubbert Geomechanics Laboratory, Department of Earth and Atmospheric Sciences, Purdue University,  
West Lafayette, IN 47907 (U.S.A.)*

(Received April 5, 1988; revised version accepted October 7, 1988)

## Abstract

Cruikshank, K.M., Neavel, K.E. and Guo Zho Zhao, 1989. Computer simulation of growth of duplex structures. *Tectonophysics*, 164: 1–12.

The geometry of hinterland-dipping duplex structures, produced by deformation over several successive ramp faults, can be explored using composite kinematic and mechanical models which were developed to describe the deformation in the vicinity of an isolated ramp. The composite kinematic model permits the relationships between ramp height, angle, spacing, and displacement to be calculated. A special case of hinterland-dipping duplex structures, approximately flat-topped structures, require a specific amount of displacement that depends on ramp angle, height, and spacing. The requirement is very sensitive to final ramp spacing, and relatively insensitive to displacement.

## Introduction

A common feature of many cross-sections of fold and thrust belts is a series of imbricate faults connecting either two thrust surfaces or two segments of a single thrust surface that steps between two different stratigraphic levels (Fig. 1). This class of structures was termed duplex structures by Dahlstrom (1970) and by Boyer and Elliott (1982). Such structures have been interpreted to exist in fold and thrust belts in Scotland (e.g. Elliott and Johnson 1980; Fisher and Coward 1982; Coward 1984), the Appalachians (e.g. Harris and Milici, 1977; Harris et al., 1981) (Fig. 1), and the Canadian Rockies (e.g. Dahlstrom 1970; Farmor and Price 1976, Price 1981).

Boyer and Elliott (1982, p. 1200) named three types of duplex structure based on geometrical form: *hinterland-dipping duplex*, *stacked duplex* and *foreland-dipping duplex* structure (Fig. 2). Hinterland-dipping and stacked duplex (antiformal stack) structures have been inferred to exist in fold and thrust belts (e.g. Charlesworth and

Gagnon 1985) and in accretionary prisms of subduction zones (e.g. Sample and Fisher 1986; Platt and Leggett, 1986).

Although the notion of the duplex structure has gained wide acceptance, and multiple thrusts are commonly interpreted to be duplex structures, the geometry of duplex structures remains largely unexplored. Suppe and Namson (1979) and Suppe (1980a, 1980b) have constructed cross-sections of antiformal stacks using a geometrical technique developed for single ramp folds. Mitra and Boyer (1986) and Mitra (1986) used geometrical relationships to classify duplex structures; however, foreland-dipping and hinterland-dipping duplex structures have not been analyzed in detail.

In this paper we concentrate on the geometry and kinematics of hinterland-dipping duplex structures (Fig. 2A). Special emphasis will be given to approximately flat-topped, hinterland-dipping duplexes (Fig. 2A), because the form of the flat-topped duplex strongly constrains the kinematic and mechanical models used to describe its development. The flat-topped duplex form also il-

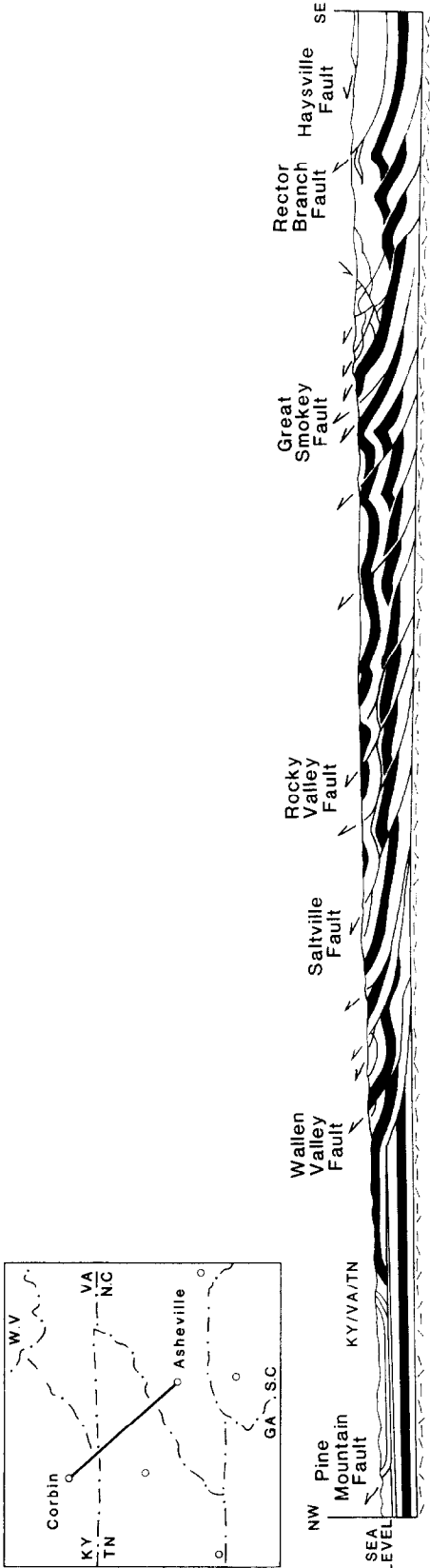


Fig. 1. Duplex structures in an interpretive cross-section, Southern Appalachians (after Kohles et al., 1985).

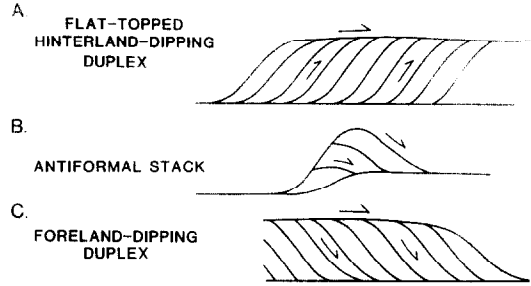


Fig. 2. The three major forms of duplex structures envisioned by Boyer and Elliott (1982, p. 1200). The antiformal stack (B) can be generated by the same kinematics as the flat-topped, hinterland-dipping duplex structure (A) with larger displacements, or a smaller ramp spacing.

illustrates the usefulness of a simple kinematic model in constructing duplex structures. A wide range of structures can be produced using the kinematic and mechanical models, from isolated ramp folds through approximately flat-topped forms to antiformal stacks, flat-topped foreland dipping structures and isolated horses on the upper thrust.

Boyer and Elliott (1982, p. 1208) presented a scenario for the formation of an idealized, flat-topped duplex structure (Fig. 3), which begins with an initial ramp fault (Fig. 3A), and involves the sequential accretion of thrust bounded packages (*horses*) to form a duplex structure (Fig. 3D). The geometry at stage two (Fig. 3B) resembles the geometry of the “fault-bend fold” of

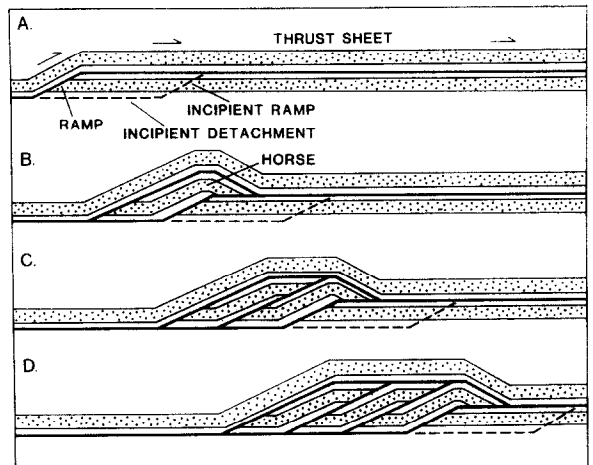


Fig. 3. Scenario for the development of a flat-topped, hinterland dipping duplex structure (after Boyer and Elliott, 1982, fig. 19, p. 1208).

Suppe (1983). Johnson and Berger (in press; Berger, 1986) have developed a kinematic model that reproduces the form of that simple fold. We will use their kinematic model, as well as the mechanical model of Berger and Johnson (1980), to investigate the geometry of approximately flat-topped hinterland-dipping duplex structures.

### A kinematic model for duplex structures

An essential tool for our analysis of duplex structures is the kinematic model of a single ramp fold (Berger, 1986). We will apply the model sequentially to a series of ramps in order to generate a duplex structure.

The elements of the kinematic model for a single ramp are shown in Fig. 4. Two detachment surfaces at different levels are connected by a ramp inclined at an angle  $\Theta$  to the detachments. The thrust sheet above the detachments is divided into three velocity domains, I, II, and III, separated by two steeply-dipping velocity discontinuities. The velocity discontinuities are oriented such that originally horizontal beds experience no change in thickness or length as the thrust sheet moves over the ramp. The velocity discontinuity originating at the base of the ramp slopes at an angle of  $\Theta/2 + 90^\circ$ , where  $\Theta$  is the ramp angle. The velocity discontinuity originating at the top of the ramp slopes at an angle of  $\gamma$  where:

$$\tan \gamma = \cot \Theta \pm [(\cot^2 \Theta) - 3]^{1/2}; \quad \Theta \leq 30^\circ \quad (1)$$

The velocity vectors are shown in Fig. 4. In each velocity domain, the velocity vector is parallel

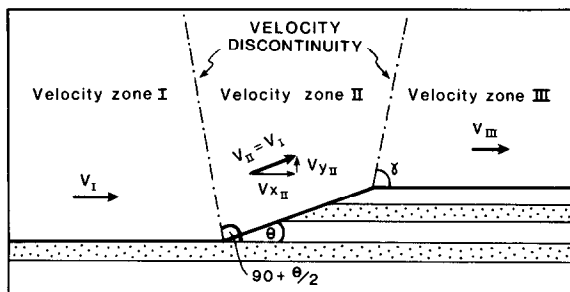


Fig. 4. Elements of the single ramp kinematic model of Berger and Johnson (1986). The thrust sheet above the ramp is divided into three velocity domains, separated by two velocity discontinuities.

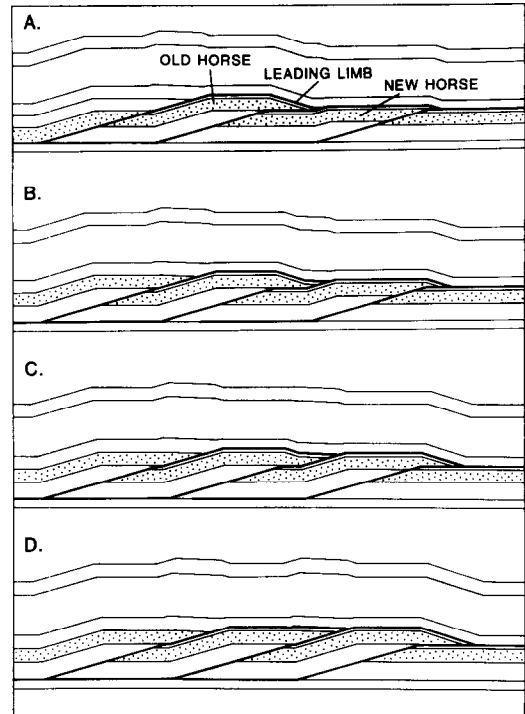


Fig. 5. Stages in a single folding event showing the accretion of a single horse. In each stage there has been further displacement to the right, the leading limb of the old horse is reoriented until it is almost horizontal. Several such events will build up a duplex structure.

to the thrust surface at the base of the domain. As a result, in zone II there are both vertical and horizontal velocity components, whereas in zones I and III there are only horizontal components. The magnitude of the velocity,  $V_I$ , is the same in zones I and II, and is lower in zone III:

$$V_{III} = V_I \frac{\sin(\gamma - \Theta)}{\sin \gamma} \quad (2)$$

Details of the development of the kinematic model and properties of the discontinuities are presented by Berger (1986).

We model the formation of a duplex structure by representing each event of ramp formation and folding with the kinematic model described above. Stages, like snapshots, in a single folding event, according to the kinematic model, are shown in Fig. 5. In each stage, the thrust sheet is pushed farther to the right.

In stage one, Fig. 5A, two ramp folds have already developed and a third is initiating, produc-

ing two horses that are completely bounded by thrust surfaces. The leading fold limb of the old horse dips in the transport direction. In order for the old horse to become an element of the flat-topped duplex structure envisioned by Boyer and Elliott (Fig. 3), its leading limb must become horizontal.

In stage two there has been further thrusting over the new detachment surface and ramp. Part of the leading limb of the old horse shown in stage one has become reoriented to a more nearly horizontal attitude. According to the kinematic model used to construct Fig. 5, the reorientation is a result of part of the leading limb passing through the first velocity discontinuity. As the leading limb passes through the discontinuity, it rotates upward. A trough has formed between the leading limb of the old horse and the trailing limb of the new horse.

During stage three there has been further thrusting, and more of the leading limb of the old horse has been reoriented.

Thrusting has stopped at the end of stage four, Fig. 5D. The leading limb of the old horse has passed through the discontinuity and is now ap-

proximately horizontal. The trough, which has nearly vanished, is represented by a shallow, highly asymmetric groove.

The concept of Boyer and Elliott (1982) for the formation of a duplex structure (Fig. 3) is modeled kinematically by a sequence of folding events such as the one shown in Fig. 5. Each succeeding event generates a new horse and reorients the leading limb of the horse formed during the previous event.

The sequence of folding events, according to the kinematic model, produces the structures shown in Fig. 6. The structure created with the kinematic model (Fig. 6) clearly is essentially the same as that envisioned by Boyer and Elliott (Fig. 3). One of the objectives of our research has thus been reached.

### Geometry of duplex structures

A specific combination of thrust displacement, ramp angle, and ramp spacing is required to produce an approximately flat-topped duplex structure such as that shown in Fig. 6. In this section we will investigate the geometry of the approxi-

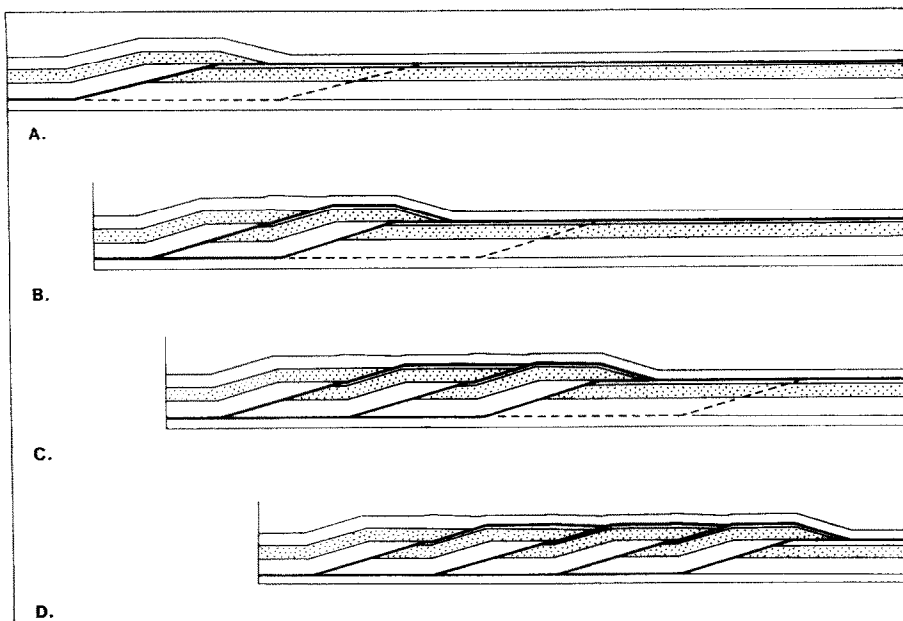


Fig. 6. A flat-topped, hinterland-dipping duplex structure generated by the composite kinematic model. The ramp angle is fifteen degrees, with a displacement of two ramp heights, and a pre-displacement ramp spacing of approximately six ramp heights. This figure should be compared with Fig. 2.

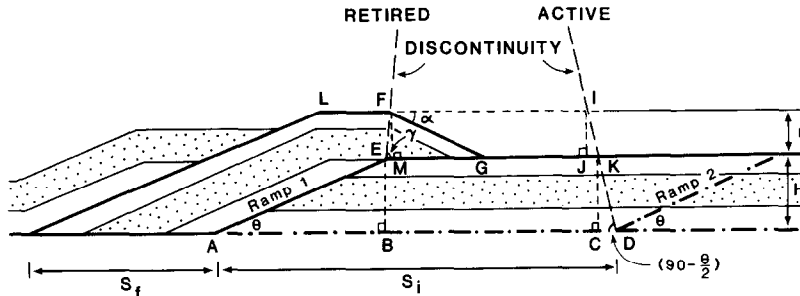


Fig. 7. Definition diagram for the critical ramp spacing required to form a duplex. Only the position of the first velocity discontinuity on ramp 2 is shown. This is at an equivalent stage to that shown in Fig. 6B.

mately flat-topped duplex structure produced by the kinematic model in order to determine relations among these factors. We have elected to solve for the final critical spacing of ramps,  $S_f$ , required to form the flat-topped duplex structure.

#### Critical spacing of ramps

The geometries of a horse, and of a block that will become a horse, are shown in Fig. 7. The situation is equivalent to that shown in Fig. 6B, just before displacement occurred on a new ramp (ramp 2, Fig. 7). The heavy lines represents segments of the thrust fault. Line segment  $FG$  represents the leading fold limb, which will become reoriented until it is parallel to the top of the structure. As indicated above, the line segment must pass through the velocity discontinuity,  $DI$  (Fig. 7).

To form a flat top, point  $F$  must reach, but not pass through, the velocity discontinuity at point  $I$ , as displacement occurs on ramp 2. Figure 8A shows the form of duplex produced if point  $F$  does not reach point  $I$ , and Fig. 8C shows the form if point  $F$  passes beyond point  $I$ . Figure 8B shows that, if point  $F$  reaches point  $I$ , the almost flat-topped form of duplex is produced.

The fixed starting and ending positions for point  $F$  (Fig. 7) required for a flat-topped duplex structure allows the calculation of a relation among ramp spacing, angle, and height, and displacement,  $U_f$ , responsible for each horse. An expres-

sion for the final ramp spacing,  $S_f$ , is derived in the appendix. The initial ramp spacing is:

$$S_i = S_f + U_f \quad (3a)$$

in which  $U_f$  is displacement of the thrust sheet, and the final ramp spacing is,

$$S_f/H = \operatorname{cosec} \Theta + U_f \{ (\sin \Theta) [1/A + \tan(\Theta/2)] \} \quad (3b)$$

where:

$$A = \tan \gamma = \cot \Theta \pm [(\cot^2 \Theta) - 3]^{1/2} \quad (3c)$$

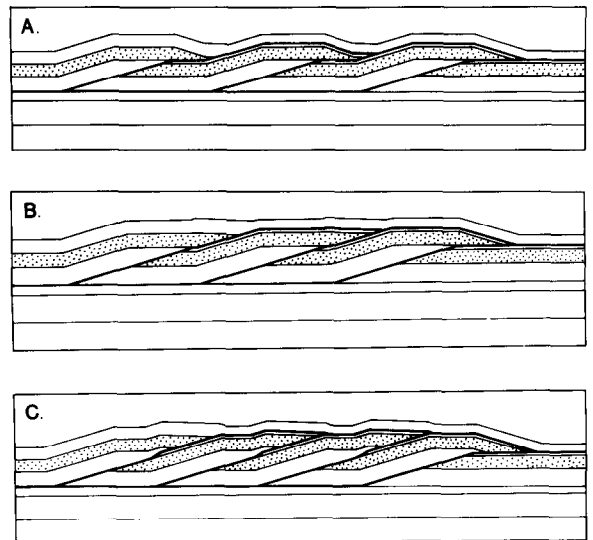


Fig. 8. The effect of displacement on the flat-topped duplex form. A. Insufficient displacement. B. The correct combination of ramp spacing and displacement. C. Displacement is too great.

Equations (3) indicate that, if the ramp angle,  $\Theta$ , displacement,  $U_I$ , and ramp height,  $H$ , are specified, the critical ramp spacing, either  $S_i$  or  $S_f$ , required for a flat-topped duplex structure, can be computed.

#### Relationship among ramp angle, ramp spacing and displacement

Figure 9 shows the relation between initial, critical ramp spacing normalized with ramp height,  $S_i/H$ , and ramp angle  $\Theta$ , for displacement equal to twice the ramp height,  $U_I/H = 2$ . Any combination of spacing and angle that plots close to the curve will result in a nearly flat-topped duplex structure. Any combination that plots above the curve will have a spacing that is too large, and the leading point of each horse will be at a lower level than the top of the most recent horse (Fig. 9A). Any combination that plots below the curve will have a displacement that is too small, and the top of the horse will be at a higher level than the top of the most recent horse (Fig. 9B).

An antiformal stack (Fig. 1B) is produced for a ramp spacing much smaller than critical. Solitary horses are produced for a ramp spacing much larger than critical.

Figure 10A shows the same relations as Fig. 9, but for several different displacement ratios,  $U_I/H$  ranging from 0.25 to 2.00. The spread of the curves reflects the sensitivity of the flat-topped

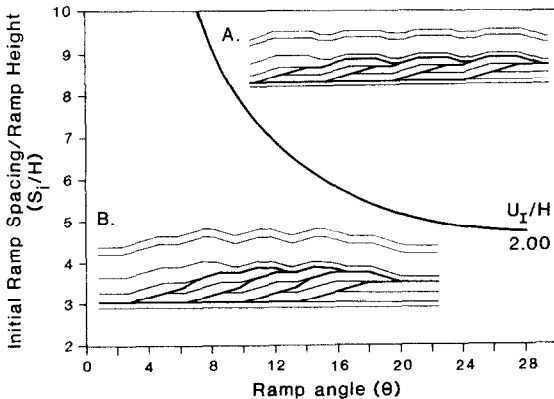


Fig. 9. Plot of ramp spacing ratio against ramp angle. The curve is for a displacement of two ramp heights. The curve separates two major geometrical domains. Stacked duplex structures plot in the lower half of the graph.

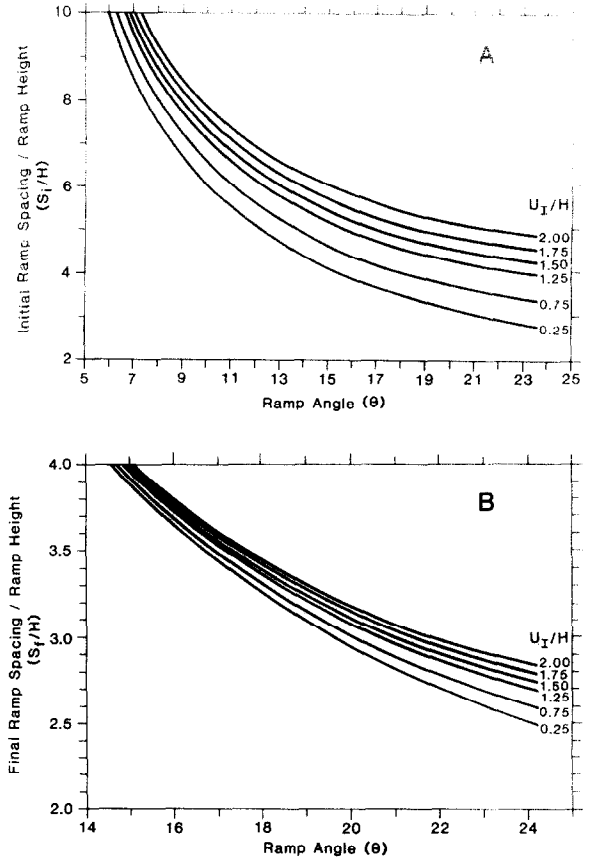


Fig. 10. Plot of the critical ramp spacing ratio against ramp angle needed to form a duplex. Curves are given for several different displacements. A. Pre-displacement ramp spacing. B. Post-displacement ramp spacing.

form to the amount of displacement. The spread is small for low ramp angles and large for high ramp angles. At low ramp angles the duplex will be essentially flat-topped over a larger range of displacement than at high ramp angles.

The graphs shown in Fig. 10 can be used to estimate an unknown parameter of a duplex structure. Figure 10A is for initial and Fig. 10B is for final ramp spacing. For example, knowing the final ramp spacing,  $S_f$ , height,  $H$ , and angle,  $\Theta$ , one can use Fig. 10B to determine the amount of displacement,  $U_I$ , responsible for each horse in an approximately flat-topped duplex structure.

#### Structural relief of a duplex structure

The structural relief ( $r$ , Fig. 7) of an approximately flat-topped duplex structure is:

$$r = U_I \sin \Theta \quad (4)$$

Equation (4) indicates that, knowing the structural relief and the ramp angle, the displacement can be determined for a flat-topped duplex structure. The maximum possible structural relief of a flat-topped duplex is equal to the ramp height.

### Discussion

We have demonstrated that a composite kinematic model for multiple ramps can reproduce the essential features of a flat-topped duplex structure and determine the geometric constraints of such structures. However, two assumptions of the basic kinematic model for a single ramp have been violated in the composite model. Application of the kinematic model derived for a single ramp to multiple ramps in duplex structures causes slight changes in bed thickness and length within the thrust sheet. This is because inclined beds pass through the velocity discontinuities. However, the composite model maintains the area of the cross-section; thus it always produces a balanced cross-section, even though the bed lengths and thicknesses change slightly.

Next we will determine whether the essential features of the flat-topped duplex can be reproduced by a composite mechanical model for bed-duplication folding in the vicinity of an isolated ramp, introduced by Berger and Johnson (1980). The mechanical model allows bed thickness and length to change, but does not allow volume to change. Thus, we violate none of the conditions used to derive the single ramp model when it is applied to multiple ramps.

### A mechanical model for duplex structures

The mechanical model of Berger and Johnson (1980; Berger, 1986) for bed-duplication folding over a single ramp will be expanded to model displacement over several successively-formed ramps. The same sequence of events will be used as in the kinematic model (Fig. 6).

The mechanical model traces the positions of passive markers in a linear-viscous block being displaced over a stepped thrust surface (Fig. 11). The thrust surface is represented by a Fourier series. The use of a large length ( $D$ , Fig. 11) allows

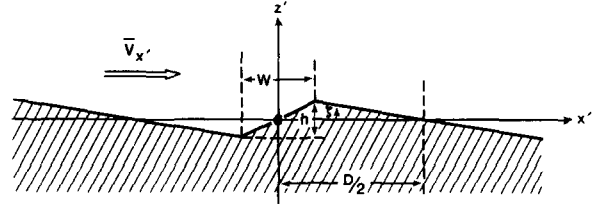


Fig. 11. Definition diagram for the Fourier series used in the analytical model.  $D$  is the wavelength,  $h$  the step height,  $W$  the step width and  $\zeta$  is the height of the interface from the  $x'$  axis.  $V_{x'}$  is the velocity of the viscous block moving over the ramp.

the deformation around a single ramp to be modeled. The final forms of the equations (to first-order), as given in Berger and Johnson (1980) and Johnson and Berger (1986), are:

$$V_{x'} = \bar{V}_{x'} + \bar{V}_{x'} \sum_{n=1}^{\infty} (A_n l_n) (l_n z') \times \exp(-l_n z') \sin(l_n x') \quad (5a)$$

$$V_{z'} = \bar{V}_{z'} \sum_{n=1}^{\infty} (A_n l_n) (l_n z' + 1) \times \exp(-l_n z') \cos(l_n x') \quad (5b)$$

where:

$$A_n = \left[ h / (n\pi)^2 \right] (D/w) [D / (D - w)] \times \sin(n\pi w / D) \quad (6a)$$

$$l_n = n\pi / D \quad (6b)$$

$V_{z'}$  and  $V_{x'}$  are the velocity components of any material particle at point  $(x, z)$ ,  $\bar{W}_{z'}$  and  $\bar{V}_{x'}$  are the mean velocities,  $w$  is the step width, measured parallel to the  $x$ -axis,  $D$  is the ramp spacing,  $S$  is the step height, and  $n$  is the number of terms in the Fourier series. The displacements of points on bedding planes are calculated by performing a fourth-order, Runge-Kutta integration of eqn. (5) (Gerald and Wheatley, 1985).

The composite mechanical model also can produce an approximately flat-topped duplex structure. The structures formed by the composite kinematic and mechanical models are fundamentally the same, as shown in Figs. 12A and 12B. The folds in the mechanical model are rounded, whereas those in the kinematic model are angular. Beds in the mechanical model thicken and thin more than those in the kinematic model. The

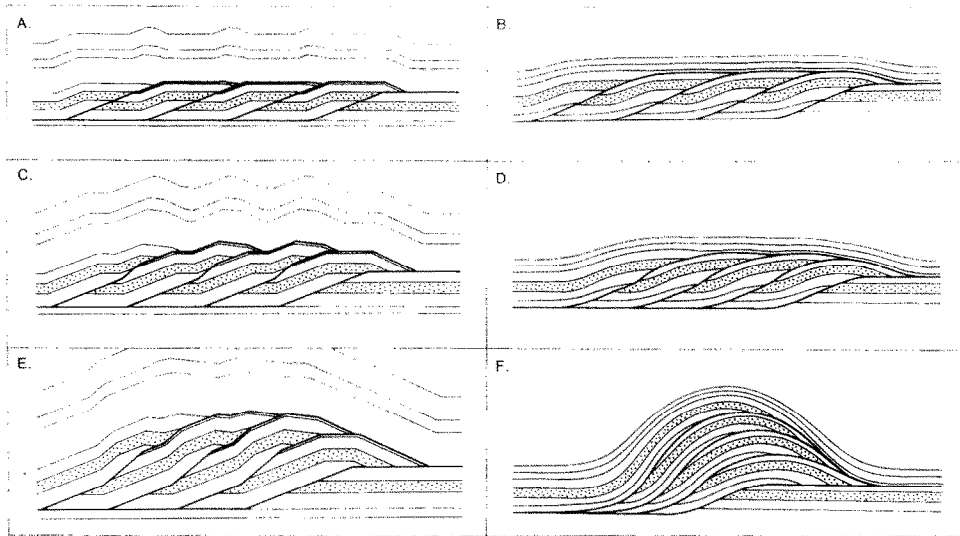


Fig. 12. Comparison between the kinematic and mechanical models. A and B show the duplex form produced by each model; C and D show the development of a stacked duplex with increasing displacement; E shows a form similar to Fig. 4C; F is the stacked duplex form.

composite mechanical model also produces a complete range of structures, from the flat-topped duplex (Fig. 12B) to the stacked duplex (Fig. 12F).

An inappropriate result of the composite kinematic model is folding of bedding in the thrust sheet high above the roof fault of the duplex structure. The small folds are particularly obvious in the bedding overlying the duplex structures shown in Figs. 12A and 12C. According to the mechanical model, small folds will occur immediately only over the duplex structure because localized disturbances must die out exponentially (eqn. 5).

### Discussion

Our composite kinematic model cannot form a duplex structure with a perfectly horizontal roof fault. The kinematic model for a single ramp produces a fold form in which the leading limb is steeper than the trailing limb (Suppe, 1983; Berger, 1986), and the steepening of the leading limb increases with ramp angle. The composite kinematic model is unable to reorient the leading limb to horizontal by passing the limb through a velocity discontinuity (as shown in the Appendix).

The composite mechanical model cannot form a perfectly horizontal roof fault in a duplex struc-

ture (Fig. 12B) for essentially the same reason. The leading limb is too steep to be reoriented to horizontal. However, at low ramp angles the roof fault is essentially horizontal in both the kinematic and mechanical models (Figs. 12A and 12B).

For example, for a ramp angle of  $30^\circ$ , which is the upper limit of the kinematic model (eqn. 1), the dip of the first velocity discontinuity is  $75^\circ$  ( $90 - \Theta/2$ ) $^\circ$ , and the dip of the leading limb ( $\alpha$ , Fig. 7) is  $60^\circ$ . After the leading limb passes through the first discontinuity on the new ramp (ramp 2, Fig. 7) its dip,  $\beta$ , is  $57$ – $58^\circ$ . The final dip of the leading limb would have to be  $0^\circ$  to produce a flat-topped duplex structure. The reason the final dip is so large in this example is that the upper part of the limb reaches the velocity discontinuity shortly after the lower part of the limb. This does not allow the limb angle to change significantly.

### Conclusions

With the exception of the minor irregularities in the roof fault explained above, the composite kinematic model can reproduce a range of duplex forms previously drafted using geometrical techniques. The composite kinematic model is based on the kinematic model of Johnson and Berger,

which reproduces the fold form of the geometrical method introduced by Suppe (1983). The composite mechanical model is based on the single ramp model of Berger and Johnson (1980).

Both composite models reproduce the essential features of the flat-topped, hinterland-dipping duplex structure of Boyer and Elliott (1982) (Figs. 1A and 2D), consisting of a series of sigmoidal horses bounded above and below by roughly parallel detachment surfaces (Figs. 3D, 6, 8B, 12A, 12B). The kinematic model is particularly useful for determining the geometric constraints of flat-topped duplex structures. Figure 10 shows how the ramp spacing, required for a flat-topped duplex structure, is constrained by displacement, ramp angle and height. The kinematic and mechanical models can be used to construct the full range of duplex structures, from isolated horses, through approximately flat-topped duplex structures, to antiformal stacks.

### Acknowledgements

Special thanks to Arvid Johnson for his assistance with this research. Virginia Pfaff reviewed an early version of the manuscript. Lyla Messick did the drafting. This paper was improved by reviews from D.V. Wiltschko and M. Friedman.

### Appendix A

#### Introduction

Here we present a brief description of the single ramp kinematic model developed by Johnson and Berger (in press). The interested reader is referred to Berger (1986) and Johnson and Berger (in press) for a complete discussion of the model.

#### Assumptions

In the form proposed by Rich (1934), bed-duplication folding requires: (1) translation of hanging-wall rocks subparallel to the thrust surface; (2) steps or curves in the thrust surface; (3) continuous contact between hanging-wall and footwall across the detachment surface; (4) stiff (or rigid) footwall. Three requirements to constrain the

geometry were added by Suppe (1983): (5) constant length of beds; (6) planer fold limbs; (7) constant thickness of beds with planer fold limbs. Suppe assumed that the folds obey most of the rules identified by Patterson and Weiss (1966) for ideal kink bands.

#### Velocity zones

In the model (Fig. 4), the area above the thrust surface is divided into three velocity zones (I, II, and III), separated by two velocity discontinuities that form zone boundaries. Within each domain the velocities are constant. One velocity discontinuity forms a zone boundary at the base of the thrust ramp and is inclined at a clockwise angle of  $(90 + \Theta/2)^\circ$ . This domain boundary is fixed in all the kinematic models. The other discontinuity forms the domain boundary at the top of the thrust ramp and is initially inclined at a counterclockwise angle,  $\gamma$ , of somewhat less than  $90^\circ$ . Johnson and Berger show that this angle changes in orientation to  $(90 + \Theta/2)^\circ$  as the bed-duplication fold stops growing.

In each domain, the velocity vector is parallel to the detachment surface. Thus, in domain I, the velocity ( $V_1$ ) is parallel to the lower detachment; in domain II, the velocity is redirected parallel to the ramp; and in domain III, it is redirected parallel to the upper detachment. The velocity vector changes abruptly at domain boundaries.

The magnitudes of the velocity vectors are equal to  $V_0$  within domains I and II because the vectors and bedding domains both parallel the detachment surface near the domain boundary, and bed length is assumed to be conserved. In domain III, the magnitude of the velocity vector is slightly less than  $V_0 \cos \Theta$ , as shown below.

Each velocity vector in domains I and II can be decomposed into a component normal to the domain boundary ( $V_{n1}$  and  $V_{n2}$ ) and component tangential to the domain boundary ( $V_{s1}$ ,  $V_{s2}$ ). The normal components match at the domain boundary. The tangential components, however, are mismatched, and there is a change in magnitude of the tangential velocity equal to:

$$V_{s2} - V_{s1} = 2V_0 \sin(\Theta/2) \quad (\text{A1a})$$

which is approximately proportional to the slope of the ramp for small slopes:

$$V_{s_{II}} - V_{s_I} \approx V_0 \tan \Theta; \quad \text{small } \Theta \quad (\text{A1b})$$

For small slopes therefore, the magnitude of the vertical velocity over the ramp is merely equal to the velocity required to lift the material up as it is transported over the ramp.

Within domain III, the velocity vector is parallel to the upper detachment, so at the boundary between zones II and III there is a change from a field of horizontal and vertical velocities to a field of horizontal velocity. The elimination of the vertical velocity component as beds cross the zone boundary causes tilting of the beds and the formation of the distal limb of a fold.

The magnitude of the velocity discontinuity at the boundary between domains II and III is determined in the same way as described above. Each vector is decomposed into normal and tangential velocity components. As a consequence, there is a discontinuity of the tangential velocity equal to:

$$V_{s_{III}} - V_{s_{II}} = V_{III} \cos \gamma - V_0 \cos(\gamma - \Theta) \quad (\text{A2a})$$

for small slope angles:

$$V_{s_{III}} - V_{s_{II}} \approx -V_0 \tan \Theta; \quad \text{small } \Theta \quad (\text{A2b})$$

Comparison of eqn. (A1b) and (A2b) shows that, for low ramp slopes, the first velocity discontinuity introduces and the second velocity discontinuity cancels the upward velocity component in the segments of material riding over the ramp fault.

#### *Relations between velocities and slopes of velocity discontinuities*

The kinematic model provides enough information to trace marker lines as they are translated across the domains of the velocity field and through the velocity discontinuities. For example, a horizontal line segment that begins in zone I will deform into a dipping line segment as it enters zone II, with a dip equal to that of the thrust ramp. Similarly, a horizontal line segment that begins in zone II and enters zone III deforms into

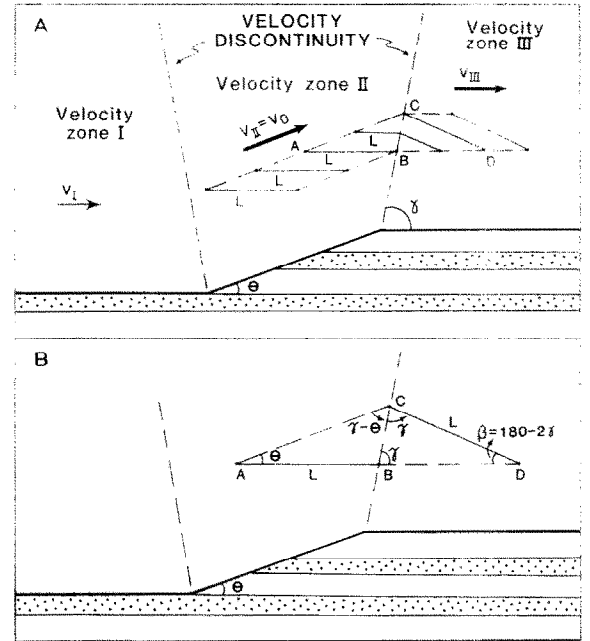


Fig. 13. Reorientation of a line,  $L$ , passing through the second velocity discontinuity in the single-ramp kinematic model (after Johnson and Berger, in press).

a line segment with a dip opposite to that of the thrust ramp.

This process is illustrated in Fig. 13A, where a single line segment,  $L$ , moves with the flow, in five time steps, from zone II across the domain boundary into zone III. The two dashed lines in Fig. 13A show displacement paths of points that mark the ends of the line.

Figure 13B shows the initial and final positions of the line segment,  $L$ , as it begins (line  $AB$ ) and completes (line  $CD$ ), its passage through the velocity discontinuity (line  $BC$ ). Points  $A$ ,  $B$ ,  $C$ , and  $D$  are shown for reference in Fig. 13A. Note that point  $A$ , at the left-hand end of the line segment, remains in domain II and point  $B$ , at the right-hand end of the line segment, remains in domain III during the entire time period,  $t$ , required for the line segment to pass through the discontinuity. As a result the length of the dashed line,  $AC$ , is:

$$AC = V_{II}t = V_0t \quad (\text{A3a})$$

similarly, the length of the dashed line  $BD$  is:

$$BD = V_{III}t \quad (\text{A3b})$$

The value of  $V_{III}$  will be determined below in terms of the velocity  $V_0$  and the slope angle,  $\Theta$ , of the ramp.

We first determine the angle,  $\gamma$ , the slope angle of the velocity discontinuity between zones II and III. Following Suppe (1983), we assume that the line element  $L$  does not change length as it passes through the zone boundary, thus:

$$AB = CD \quad (A4a)$$

Following Patterson and Weiss (1966), we assume that beds are the same thickness on either side of the zone boundaries, or as shown in Fig. 13B.

$$\angle DBC = \angle DCB \quad (A4b)$$

The two assumptions stated above, (A4a) and (A4b), complete the definition of the geometry shown in Fig. 13B, and from the geometry, we can eliminate the unknowns:

Considering triangle  $BCD$ , and using the law of sines:

$$\sin(180 - 2\gamma)/BC = (\sin \gamma)/L \quad (A5a)$$

Considering triangle  $ABC$ :

$$(\sin \Theta)/BC = \sin(\gamma - \Theta)/1 \quad (A5b)$$

The unknown length  $BC$  can be eliminated between eqn. (A5), using trigonometric identities, and then the side length of a hypothetical right-triangle continuing  $\gamma$  in order to derive the following result:

$$\tan \gamma = \cot \Theta \pm [(\cot^2 \Theta) - 3]^{1/2}; \quad \Theta \leq 30^\circ \quad (A-6)$$

This is eqn. (1) in the main text. Equation (A6) generally has two real roots. For  $\Theta = 30^\circ$  however, it has only one:

$$\tan \gamma = \cot \Theta - \tan(90 - \Theta)$$

$$\gamma = 60^\circ; \quad \Theta = 30^\circ,$$

For ramp angles greater than  $30^\circ$ , the roots of eqn. (A6) are imaginary, so there is no orientation of discontinuity that will satisfy the conditions of zero lengthening and thickening of beds.

The relation between the velocities in domains I and II on the one hand and zone III on the other

can be derived with the law of sines, using angles  $ABC$  and  $BCA$  shown in fig. 13B.

$$\sin(\gamma - \Theta)/L = \sin(180 - \Theta)/AC \quad (A7a)$$

which according to eqn. (3b), can be written:

$$\sin(\gamma - \Theta)/V_{III}t = \sin(180 - \gamma)/V_0t \quad (A7b)$$

because  $BD = L$ . Thus:

$$V_{III} = V_0 [\sin(\gamma - \Theta)/\sin \gamma] \quad (A8a)$$

or:

$$V_{III} = V_0 (\cos \Theta - \sin \Theta \cot \gamma) \quad (A8b)$$

Thus eqns. (A6) and (A8) provide the necessary relations for determining the slope angle of the second discontinuity and the magnitude of the velocity vector within domain III.

## Appendix B

Here we present derivations of the equation for the critical ramp spacing required to approximate a flat-topped duplex structure (eqn. 3, in text) and the equation for the final orientation of a line passing through the first velocity discontinuity.

### Critical ramp spacing

According to Fig. 7, the critical final ramp spacing ( $S_f$ ) is:

$$S_f = AB + EM + JK + CD \quad (B1)$$

Using right triangle ABE:

$$AB = H \cot \Theta \quad (B2)$$

where  $H$  is the ramp height and  $R$  is ramp angle.

Considering right triangle  $EFM$ :

$$FM = U_j \sin \Theta \quad (B3)$$

thus:

$$EM = U_j \sin \theta \cot \gamma \quad (B4)$$

Using the right triangle  $IJK$  and the relationship  $IJ = FM$ :

$$JK = U_1 \sin \Theta \tan(\Theta/2) \quad (B5)$$

Finally, from right triangle  $KCD$ :

$$CD = H \tan(\Theta/2) \quad (B6)$$

Substituting eqns. (B2)–(B6) into eqn. (B1) and combining terms:

$$S_i/H = \cot \Theta + \tan(\Theta/2) + (U_i/H \sin \Theta)[\cot \gamma + \tan(\Theta/2)] \quad (\text{B7})$$

This is equivalent to eqns. (3) in the text.

*Reorientation of a line passing through the first velocity discontinuity*

The dip,  $\alpha$ , of the leading limb of the most recent horse will have a new dip,  $\beta$ , after passing through the velocity discontinuity. By considering the geometry before and after the leading limb passes through the discontinuity (allowing the length of the limb to change), we derive the following relationship between  $\alpha$ ,  $\beta$ , and  $\Theta$ :

$$\frac{\cos(\Theta/2 + \alpha)}{\sin \alpha} = \frac{\cos(\Theta/2 + \beta)}{\sin(\Theta + \beta)} \quad (\text{B8})$$

Solving for  $\beta$  in terms of the ramp angle,  $\Theta$ , and the original dip of the limb,  $\alpha$ , gives:

$$\cot(\Theta + \beta) = \cot \alpha - 2 \tan(\Theta/2) \quad (\text{B9a})$$

or:

$$\beta = -\Theta + \cot^{-1}[\cot \alpha - 2 \tan(\Theta/2)] \quad (\text{B9b})$$

## References

- Berger, P., 1986. An analysis of bed duplication folding. Doct. Diss. Department of Geology, University of Cincinnati (unpublished).
- Berger, P. and Johnson, A.M., 1980. First-order analysis of deformation of a thrust sheet moving over a ramp. *Tectonophysics*, 70: T9–T24.
- Boyer, S.E. and Elliott, D., 1982. Thrust Systems. *Am. Assoc. Pet. Geol. Bull.*, 66: 1196–1230.
- Charlesworth, H.A.K. and Gagnon, L.G., 1985. Intercutaneous wedges, the triangle zone and structural thickening of the Mynheer coal seam at Coal Valley in the Rocky Mountain Foothills of central Alberta. *Bull. Can. Pet. Geol.*, 33: 22–30.
- Coward, M.P., 1984. A geometrical study of the Arnaboll and Heilam thrust sheets, NW of Ben Arnaboll, Sutherland. *Scott. J. Geol.*, 20: 87–106.
- Dahlstrom, C.D.A., 1969. Balanced cross sections. *Can. J. Earth Sci.*, 6: 743–757.
- Dahlstrom, C.D.A., 1970. Structural geology in the eastern margin of the Canadian Rocky Mountains. *Bull. Can. Pet. Geol.*, 18: 332–406.
- Elliott, D. and Johnson, M.R.W., 1980. The structural evolution of the northern part of the Moine thrust zone. *Trans. R. Soc. Edinburgh*, 71: 69–96.
- Fermor, P.R. and Price, R.A., 1976. Imbricate structures in the Lewis thrust sheet around Cate Creek and Haig Broog windows, southeast British Columbia. *Can. Geol. Surv. Pap.*, 76-1B:7–10.
- Fischer, M. and Coward, M.P., 1982. Strains and folds within thrust sheets: an analysis of the Heilam sheet, northwest Scotland. *Tectonophysics*, 88: 291–312.
- Gerald, C.F. and Wheatley, P.O., 1985. *Applied Numerical Analysis*. Addison-Wesley, Menlo Park, Calif., 3d edn.
- Harris, L.D. and Milici, R.D., 1977. Characteristics of thin-skinned style of deformation in the southern Appalachians and potential hydrocarbon traps. *U.S. Geol. Surv., Profess. Pap.*, 1018.
- Harris, L.D., Harris, A.G., De Witt, Jr., W. and Bayer, K.C., 1981. Evaluation of southern Eastern Overthrust Belt beneath Blue Ridge-Piedmont thrust. *Am. Assoc. Pet. Geol., Bull.*, 65: 2497–2505.
- Johnson, A.M. and Berger, P., in press. Fault-bend folds. *Eng. Geol.*
- Kohles, K.M., Rast, N., Trimble, D.C. and Neavel, K.E., 1985. The Pineville–Hot Springs Section, Kentucky and Tennessee. In W.B. Woodward (Editor), *Valley and Ridge Thrust Belt: Balanced Structural Sections, Pennsylvania to Alabama*. *Univ. Tennessee Stud. Geol.*, 12: 64 pp.
- Mitra, G., and Boyer, S.E., 1986. Energy balance and deformation mechanisms of duplexes. *J. Struct. Geol.*, 8 (3/4): 291–304.
- Mitra, S., 1986. Duplex structures and imbricate thrust systems: geometry, structural position, and hydrocarbon potential. *Am. Assoc. Pet. Geol. Bull.*, 70 (9): 1087–1112.
- Patterson, M.S. and Weiss, L.E., 1966. Experimental deformation and folding in phyllite. *Geol. Soc. Am. Bull.*, 77: 343–374.
- Platt, J.P. and Leggett, J.K., 1986. Stratal extension in thrust footwalls, Makran accretionary prism: implications for thrust tectonics. *Am. Assoc. Pet. Geol. Bull.*, 70: 191–203.
- Price, R.A., 1981. The Cordilleran foreland fold and thrust belt in the southern Canadian Rocky Mountains. In: K.R. McClay and N.J. Price (Editors), *Thrust and Nappe Tectonics*. *Spec. Publ. Geol. Soc. London*, 9: 427–488.
- Rich, J.L. 1934. Mechanics of low angle overthrust faulting as illustrated by Cumberland thrust block, Virginia, Kentucky, and Tennessee. *Am. Assoc. Pet. Geol. Bull.*, 18: 1584–1596.
- Sample, J.C. and Fisher, D.M., 1986. Duplex accretion and underplating in ancient accretionary complex, Kodiak Islands, Alaska. *Geology*, 14: 160–163.
- Suppe, J., 1980a. A retrodeformable cross section of northern Taiwan. *Proc. Geol. Soc. China*, 23: 46–55.
- Suppe, J., 1980b. Imbricated structure of western foothills belt, southcentral Taiwan. *Pet. Geol. Taiwan*, 17: 1–16.
- Suppe, J., 1983. Geometry and kinematics of fault-bend folding. *Am. J. Sci.*, 283: 648–721.
- Suppe, J. and Namson, J., 1979. Fault-bend origin of frontal folds of the western Taiwan fold and thrust belt, 1. *Pet. Geol. Taiwan*, 16: 1–18.